

Semi-empirical and semi-quantitative lightweight shielding design algorithm

Song-Chuan Zheng¹, Qing-Quan Pan (<https://orcid.org/0000-0002-9384-0070>)^{2*},

Huan-Wen Lv³, Song-Qian Tang³, Xiao-Jing Liu^{1*}

1. College of Smart Energy, Shanghai Jiao Tong University, Shanghai 200240, China

2. School of Nuclear Science and Engineering, Shanghai Jiao Tong University, Shanghai 200240, China

3. Science and Technology on Reactor System Design Technology Laboratory, Nuclear Power Institute of China, Chengdu 610200, China

Corresponding Author, panqingquan@sjtu.edu.cn; xiaojingliu@sjtu.edu.cn

This work is sponsored by Natural Science Foundation of Shanghai (No. 22ZR1431900) and the Young Elite Scientist Sponsorship Program of the China National Nuclear Corporation (CNNC).

ABSTRACT

The lightweight shielding design of small reactors is a popular research topic. Based on a small helium-xenon-cooled solid reactor, the effects of neutron and photon shielding sequence and the number of shielding layers on the radiation dose were first studied. It was found that when photons were shielded first and the number of shielding layers was odd, the radiation dose could be significantly reduced. To reduce the weight of the shielding body, the relative thickness of the shielding layers was optimized using the genetic algorithm. The optimized scheme can reduce the radiation dose by up to 57% and reduce the weight by 11.84%. To determine the total thickness of the shielding layers and avoid the local optimal solution of the genetic algorithm, a series of formulas that describes the relationship between the total thickness and the radiation dose was developed through large-scale calculations. A semi-empirical and semi-quantitative lightweight shielding design algorithm is proposed to integrate the above shielding optimization method that verified by the Monte Carlo method. Finally, a code, SDIC1.0, was developed to achieve the optimized lightweight shielding design for small reactors. It was verified that the difference between the SDIC1.0 and the RMC code is approximately 10% and that the computation time is shortened by 6.3 times.

Keywords: Small reactor; Lightweight; Shielding calculation; Genetic algorithm

1. INTRODUCTION

Owing to the particular applications of small reactors, there are significant requirements for their mobility and safety, which strictly limit the size and weight of the reactor. Therefore, lightweight shielding designs are vital for small reactors. The

lightweight shielding design of small reactors is mainly based on the selection of materials and arrangement of the shielding layers. The purpose is to determine a shielding scheme that is lightweight, small in volume, and excellent in terms of the shielding effect.

Multiple parameters, such as mass, volume, and radiation dose, must be balanced in lightweight shielding design [1-3]. The Monte Carlo method can effectively address complex shielding problems with complex structures, nonuniformity, and strong anisotropy. Many reactor shielding designs based on the Monte Carlo method have been performed [4-7]. Applying the Monte Carlo method to shielding design based on traditional experience is unreasonable because of low efficiency and high design costs. It is challenging to meet the requirements of the shielding design of small reactors. When the thickness of the shielding layer exceeds a specific range, the deep penetration problem [8-9] causes the calculation result of the Monte Carlo method to deviate significantly from the theoretical value [10], so it is difficult to converge [11-12].

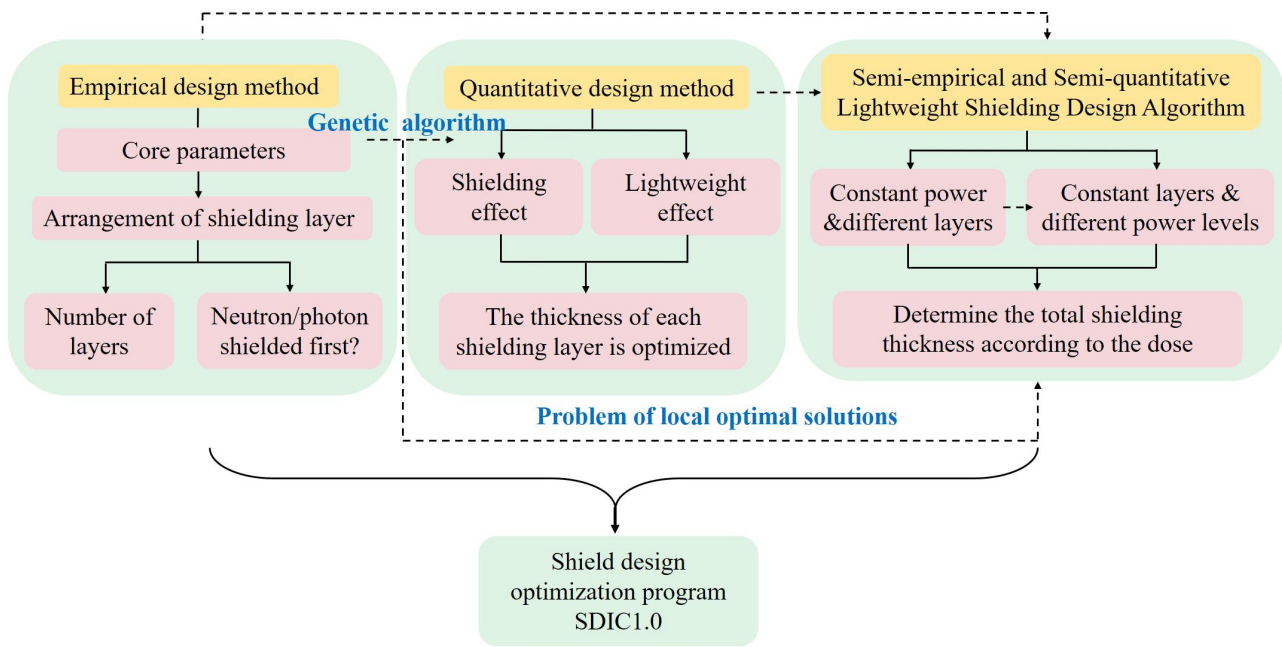
Various optimization algorithms have been proposed to improve the efficiency of lightweight shielding design. With the rapid development of optimization algorithms, some scholars have used related algorithms in shielding design [13-15]. Intelligent optimization algorithms, such as the genetic algorithm (GA) [16-17], particle swarm optimization (PSO) [18], and neural network algorithms [19], are typically heuristic. Setting appropriate optimization parameters can reduce the time required for optimization. These algorithms have been widely used in the development of shielding material [20] and optimization of shielding component [21]. The reactor shielding optimization method based on the above algorithms can improve computational efficiency.

Nevertheless, when the parameter settings are not reasonable, general heuristic algorithms can easily generate local optimal solutions. At this time, it cannot be

verified if the generated optimal solutions are global [22] or if they waste resources in the actual design stage. There are two fundamental methods to avoid the generation of local optimal solutions [23]. The first method is an in-depth study of the mechanism of the problem. By establishing a problem-based mathematical equation, the extreme value of the equation can be determined, or the characteristics of the equation can determine the interval where the extreme value is located. The second method is a random search. For discrete problems, the probability of local optimal solutions can be reduced by increasing the randomness of the search range. Standard random search methods, such as roulette, Gaussian mutation, Cauchy mutation, and “Gauss-Cauchy” mixed mutations, have been widely used [24]. However, regardless of the above methods, when the model is too complex, the amount of information processed is too large, the generation of local optimal solutions cannot be avoided entirely.

In this study, an empirical shielding design method was established to determine the number of shielding layers and order of neutron/photon shielding through a series of numerical simulation calculations. Subsequently, the GA was used to optimize the relative thickness of the shielding layers. Finally, we established the relationship between the total thickness of the shielding layer and the dose by a large number of calculation under different power ranges. Based on this relationship, a quantitative shielding design method is proposed. Before the relative thickness of each layer is optimized by the GA, this method can provide a quantitative solution for the total thickness of the shielding layer according to the power and core design parameters. The generation of local optimal solution can be avoided in the optimization of the GA by considering the quantitative solution and the dose limit as constraints for algorithm optimization. The Reactor Monte Carlo (RMC) software was used to verify the accuracy of the above method in terms of the shielding and weight reduction effects. The results show that based on the semi-empirical and semi-quantitative lightweight shielding design method, the shielding scheme can be quickly determined to achieve

the design goal of reducing the weight of the shielding layer. The remainder of this



paper is organized as illustrated in Figure 1.

Fig. 1 Structure of this paper.

2. EMPIRICAL SHIELD DESIGN METHOD

2.1 Core design and source characteristics

The shielding design was performed based on a small helium xenon-cooled reactor, as shown in Figure 2. The internal geometric unit of the core has a repetitive hexagonal structure. The entire core is built with 1040 fuel rods with a diameter of 1.5 cm, surrounded by six coolant channels with a diameter of 0.8 cm. The overall radius of the core is 44 cm, the total height is 100 cm, and the design power is 20 MW.

The core is made of graphite as the base material, the fuel rods are filled with UC composed of uranium with an enrichment ratio of 19.75%, and the coolant cladding is made of Titnium-Zirconium-Molybdenum (TZM) alloy. The core is wrapped with a 20 cm thick Be reflective layer. B₄C is a functional ceramic material with excellent properties, especially a high thermal neutron absorption capacity, the neutron shielding material selected in this study is B₄C. Stainless steel contains iron and is widely used for photon shielding. We selected SS-316 stainless steel as the photon-shielding material.

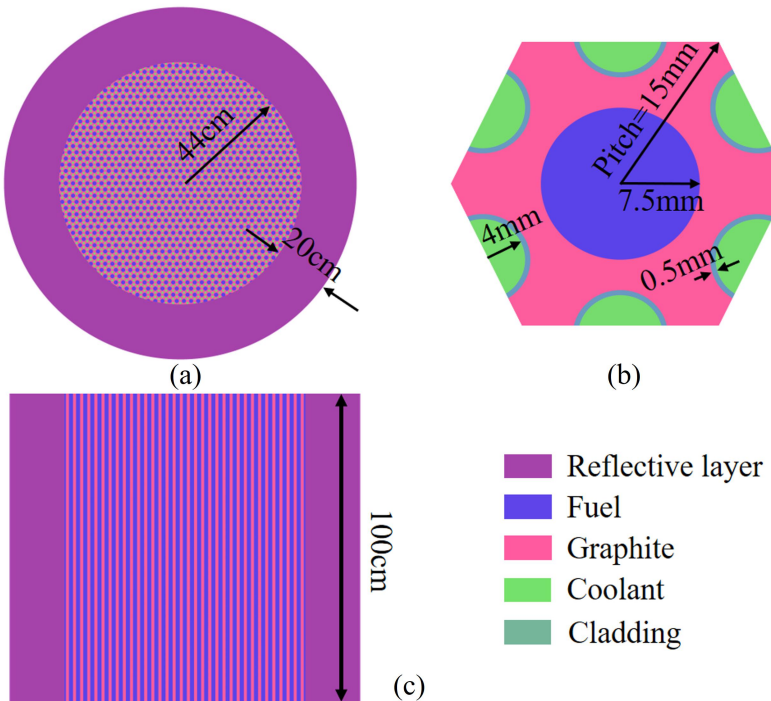


Fig. 2 (Color online) Small helium xenon-cooled reactor. (a) Top view of the

core. (b) Structural unit of a fuel rod. (c) Front view of the core.

We defined the reactor source term as a volume source. For a reactor with a specified design power, when operating at full power conditions, the energy released by each fission is 180.912 MeV, where $1 \text{ MeV} = 1.602 \times 10^{-13} \text{ J}$. Thus, the amount of nuclear fission required to produce 1 J of heat was calculated as follows:

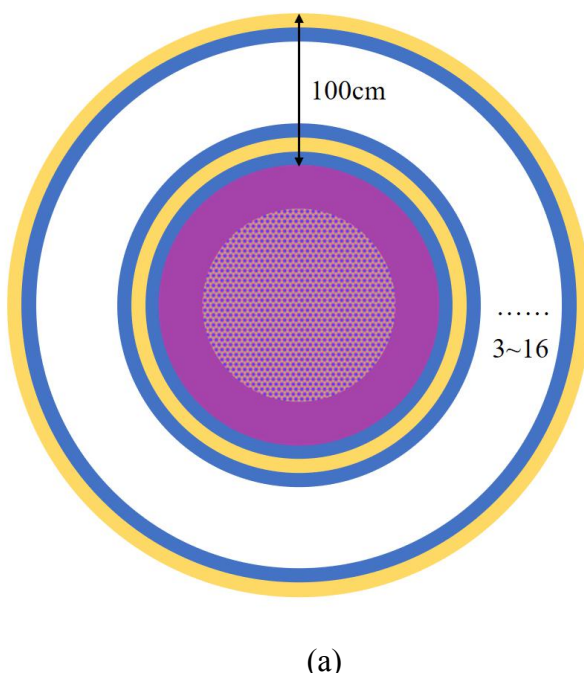
$$\frac{1 \text{ Mev}}{1.602 \times 10^{-13} \text{ J}} \times \frac{1 \text{ fission}}{180.902 \text{ Mev}} = 3.45041 \times 10^{10} \text{ fission/J}. \quad (1)$$

We assumed that the number n of neutrons produced by each fission is 2.45. If $k_{\text{eff}} = 1$, then every 2.45 source neutrons provided by the core will undergo a fission (the remaining fission neutrons are absorbed or escaped). The physical meaning of the above process is the number of fission neutrons required for every 1 J of energy released by the system per unit of time. If the power is P , then the source intensity A is calculated as follows:

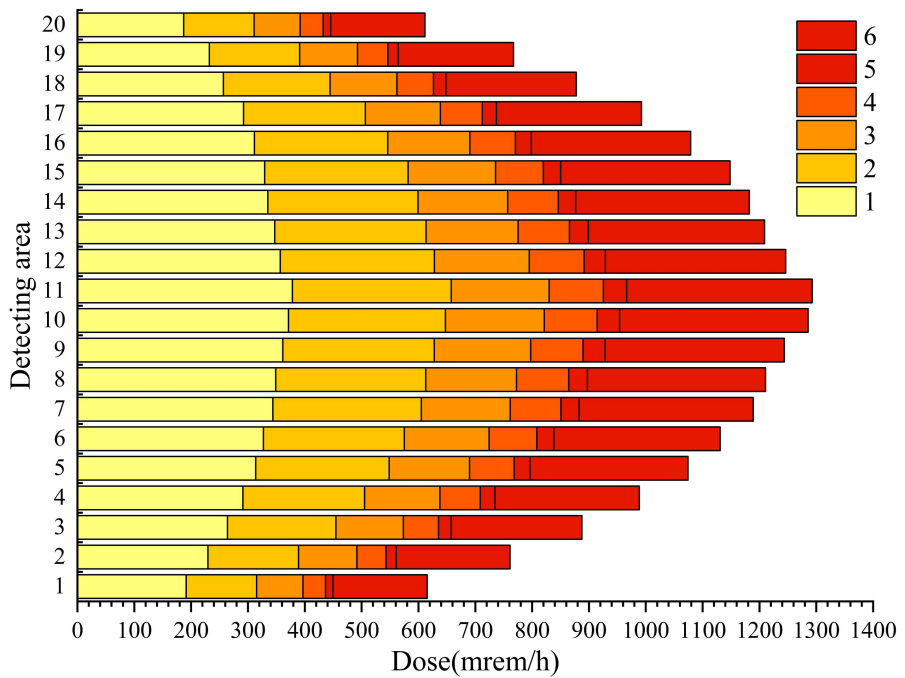
$$A = P \times 3.4504 \times 10^{10} \times n = 1.69 \times 10^{18}. \quad (2)$$

2.2 Basic shielding schemes with empirical method

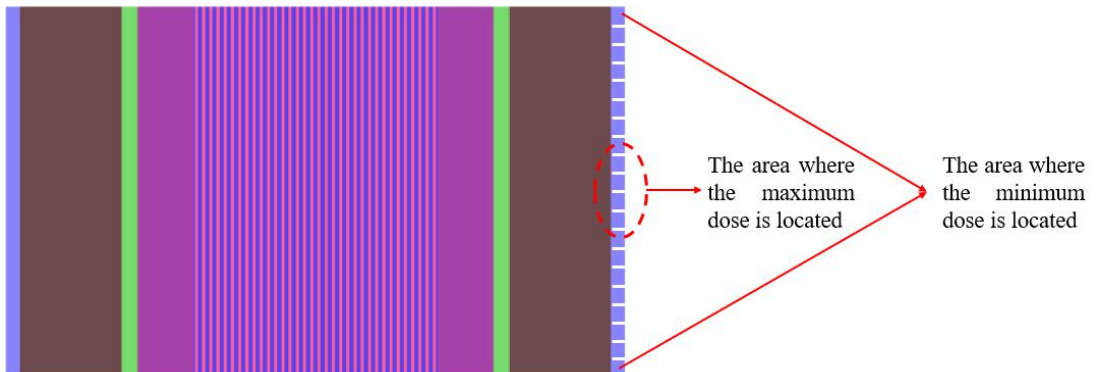
As shown in Figure 3(a), the total thickness of the shielding layer was set to 100 cm, and the thickness of each layer remained the same. We increased the number (limited to 3-16) of shielding layers to explore the variation law of radiation dose rate.



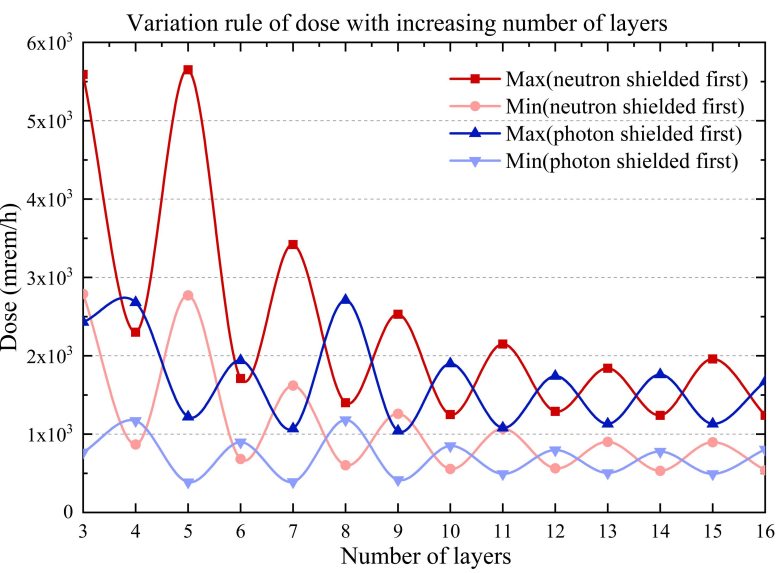
(a)



(b)



(c)



(d)

Fig. 3 (Color online) Determination of empirical shielding design scheme. (a) Initial shielding scheme. (b) Distribution law of radial dose along the axial direction. (c) Areas where dose extrema may locate. (d) Variation rule of dose with the increasing number of layers.

The schemes were further classified according to the sequence of shielding order for neutrons and photons. The statistical results for a large number of particles were the same as those for a large-scale repeated simulation of a single particle under the same conditions. However, with a continuous increase in the number of particles, it is not guaranteed that all particles will eventually be captured or absorbed by the shielding material, and some of the particles will pass through the shielding layer to reach the outer vacuum boundary. Therefore, by setting the detection area and counting the radiation dose within the area, the design scheme of the shielding layer can be evaluated. The dose was not uniformly distributed along the axis. To improve the statistical accuracy, a circle of air with a thickness of 5 cm was added at the periphery of the shielding layer to be the detection area, and 20 areas were uniformly divided along the axis, with a total height of $20 \times 5 \text{ cm} = 100 \text{ cm}$. As shown in Fig. 3(b), we calculated the dose in each area and determined the distribution law of the radial dose (mrem/h) in 20 areas along the axial direction of the six trial plans. Statistics show that the maximum dose value appears in the middle area, and the minimum value appears at the two ends, as shown in Fig. 3(c). Shielding calculations were performed using the Monte Carlo software RMC. The variation law of the maximum/minimum radiation dose in the obtained detection area with the number of layers and order of particle shielding is shown in Fig. 3(d).

As shown in Fig. 3(d), with the same total thickness, if the neutrons were shielded first (NSF), the dose rate and number of shielding layers were negatively correlated and ultimately converge to a certain range. Moreover, the radiation dose rate is lower when the total number of layers is even. If the photons were shielded

first (PSF), with an increase in the number of shielding layers, the dose rate did not evidently decrease or converge. The dose rate was relatively low when the number of layers was odd. Compared to the scheme with the same number of layers and shielding neutrons first, the dose was reduced by 3–5 times. The dose difference between the odd and even numbers of shielding layers must be explained in conjunction with the particle transport process in the reactor. The scattering of neutrons in the reactor generates photons. If neutrons can be effectively shielded, it is equivalent to pre-shielding a portion of photons. For example, when neutrons are shielded first, and the number of layers is set to four, because the B₄C of the first and third layers have shielded most of the neutrons, the secondary photons generated by neutrons are small, and these photons can be absorbed by applying SS-316 to the outermost layer of the shielding body, and the dose is evidently lower than that of the three-layer shielding design with the same total thickness.

Therefore, two empirical shielding schemes were proposed: (1) Scheme I: shield photons first with an odd number of layers, and (2) Scheme II: shield neutrons first with an even number of layers.

3. QUANTITATIVE SHIELD DESIGN METHOD

3.1 Relative thickness optimization with GA

The empirical method determines the number of shielding layers and neutron/photon shielding order. These two parameters were not considered in the subsequent optimization and could be directly used as the modeling basis for the shielding body. However, the empirical method cannot optimize the relative thickness of the shielding layer because it only provides a scheme with uniform thickness. To further reduce the weight, the GA method was used to optimize the relative thickness of the shielding layers.

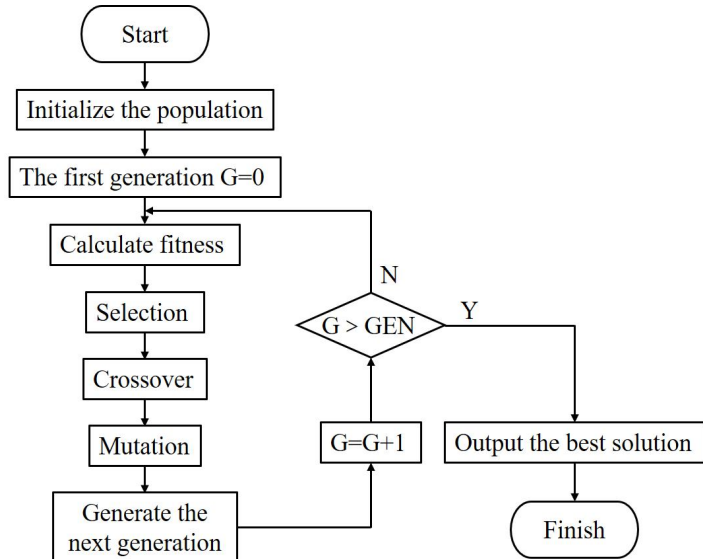


Figure. 4 GA flowchart.

The genetic manipulation of radiation shielding scheme primarily includes population selection, crossover and mutation, which are discussed separately below.

1) Selection

Suppose the group size is m and the fitness of individual i is F_i ; then, the probability P of individual i being selected is

$$P = \frac{F_i}{\sum_{i=1}^m F_i}. \quad (3)$$

2) Crossover

We used the single-point crossover operator, randomly selected a position in the paired chromosomes, and then performed locus transformation on the paired chromosomes at the selected position.

3) Mutation

To ensure the diversity of individuals, it is necessary to mutate the individual continuously in the iterative process. In this study, the single-point mutation method was adopted. That is, only a certain bit in the gene sequence needs to be mutated using binary coding as an example.

The mathematical function model for solving the optimal thickness of each layer under different layer-arrangement schemes is as follows:

$$\begin{cases} \min y = F(x) = [f_3(x), f_4(x), \dots, f_{16}(x)]^T \\ \text{s.t. } g_i(x) \leq 0, i = 1, 2, \dots, q \\ h_j(x) = r, j = 1, 2, \dots, p \end{cases} \quad (4)$$

where x is the n-dimensional design variable, $x = (x_1, x_2, \dots, x_n) \in X$, which includes the selection of shielding materials, the number of shielding layers and initial thickness of each layer. X is the design variable value space. A hybrid coding method was adopted. In other words, binary coding was used to express the order of each shielding layer in each scheme, and symbol coding was used to express the type of material assigned to a single shielding layer. Here, we chose only B₄C and SS-316 stainless steels as the shielding material input. y is the m-dimensional design objective. In this study, y includes the lowest level achieved by the maximum and minimum radiation doses in each detection area as well as the total weight of the shielding body. Simultaneously, the fitness function during the operation of the GA was determined according to the above design goals. $f_3(x) - f_{16}(x)$ represent different schemes with 3–16 shielding layers, respectively. $g_i(x) \leq 0$ defines q inequality constraints, $h_j(x) = r$ defines p equality constraints.

When the iteration stop condition is satisfied, the optimal solution can be outputted according to the fitness ranking. The shielding design problem is essentially

a multi-objective optimization problem; there will inevitably be conflicts between the various sub-objectives. To better reflect the importance of some sub-objectives, it is necessary to reasonably set the weight of each sub-objective in the fitness function. The Analytic Hierarchy Process (AHP) is adopted in this study to determine the weight of each index and select the optimal solution [25].

AHP is an efficient way to define the weights of each sub-objective in a multi-objective optimization problem. This method has the advantages of fewer information requirements and shorter decision-making time. The AHP steps are as follows.

- 1) Create a positive reciprocal matrix

$$A = (a_{ij})_{m \times m} = \begin{bmatrix} 1 & a_{12} & \cdots & a_{1m} \\ a_{21} & 1 & \cdots & a_{2m} \\ \vdots & \vdots & \ddots & \vdots \\ a_{m1} & a_{m2} & \cdots & 1 \end{bmatrix}. \quad (5)$$

where $a_{ji} = \frac{1}{a_{ij}}$, and its value is determined using Table 1. For example, the total weight of the shielding body is compared to the lowest level that can be achieved by the maximum dose in the detection area. If the former is significantly more important than the latter, then $a_{12} = 5$ and $a_{21} = \frac{1}{5}$. Each indicator was compared with other indicators, and the reciprocal matrix A was determined.

Table. 1 Scale determination of positive reciprocal matrix The values of random consistency factor RI .

Scale determination of positive reciprocal matrix																		
Scale	Criterion																	
1	Factor i is as important as factor j																	
3	Factor i is slightly more important than factor j																	
5	Factor i is significantly more important than factor j																	
7	Factor i is strongly more important than factor j																	
9	Factor i is extremely more important than factor j																	
Note: 2, 4, 6 and 8 are the intermediate values of the comparison between factor i and factor j																		
Values of random consistency factor RI .																		
m	1	2	3	4	5	6	7	8	9									
RI	0	0	0.58	0.90	1.12	1.24	1.32	1.41	1.45									

- 2) Perform a consistency check.

Normalize each column vector of matrix A as follows:

$$\tilde{w}_{ij} = a_{ij} / \sum_{i=1}^m a_{ij} . \quad (6)$$

Sum \tilde{w}_{ij} in rows to obtain $\tilde{w}_i = \sum_{j=1}^m \tilde{w}_{ij}$.

Normalize \tilde{w}_i to $\tilde{w}_i = \sum_{i=1}^m \tilde{w}_{ij}$, where $w = (w_1, w_2, \dots, w_m)^T$ is the eigenvector.

$$\text{Calculate } \lambda = \frac{1}{m} \sum_{i=1}^m \frac{(Aw)_i}{w_i} .$$

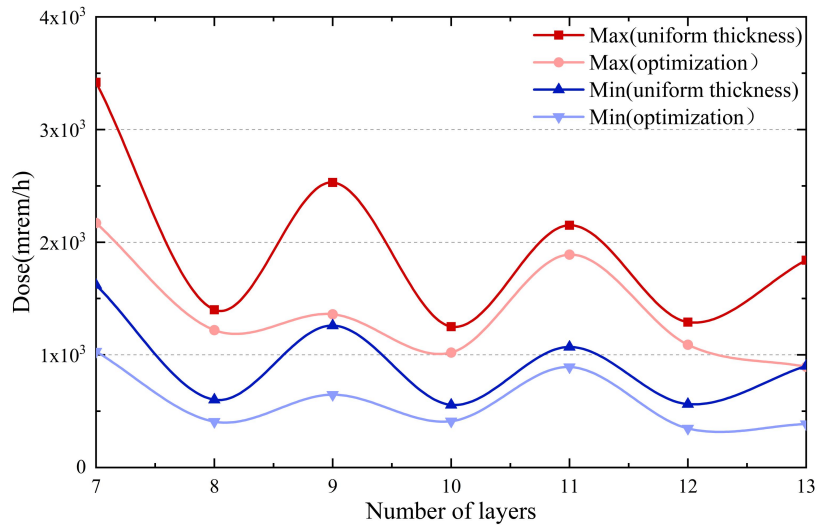
The consistency factor is given by $CI = \frac{\lambda - m}{m-1}$, where m is the order of the positive reciprocal matrix \mathbf{A} . CI is compared with the same-order random consistency factor RI in Table 1; that is, the consistency ratio is $CR = \frac{CI}{RI}$. When $CR < 0.1$, it indicates that the positive reciprocal matrix \mathbf{A} meets the consistency standard; otherwise, matrix \mathbf{A} must be properly modified. When the positive reciprocal matrix \mathbf{A} passes the consistency test, eigenvector $w = (w_1, w_2, \dots, w_m)^T$ is the required weight vector.

To improve the probability of obtaining the optimal solution, the population size was set to 50, and the evolutionary generation was 100. Previous related research have shown that when the mutation probability is greater than 0.04, the result becomes unstable; we set the mutation probability to 0.02. Simultaneously, to obtain a better local search ability, the crossover probability was set to 0.5 [26]. Schemes with 7–13 shielding layers were selected as the calculation samples, and the statistical doses under different shielding layer schemes are summarized in Table 2 (unit: mrem/h) and Fig.5.

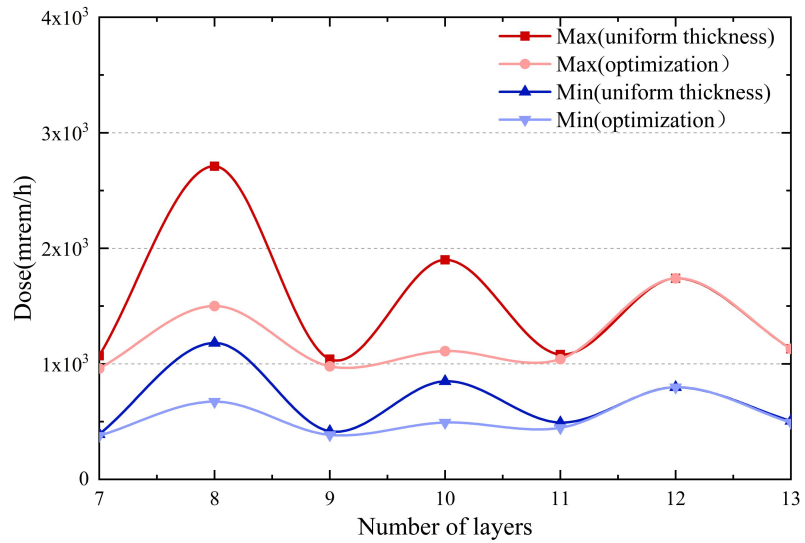
Table 2 Comparison of extreme dose values in the detection area before and after the relative thickness of each layer is optimized. (D_{um} : before optimization, that is, under the condition that the thickness of each layer is consistent, the extreme value of the

dose in the detection area, $m = 1, 2, 3, 4$; D_{vn} : the extreme value of the dose in the detection area after optimization, $n = 1, 2, 3, 4$.)

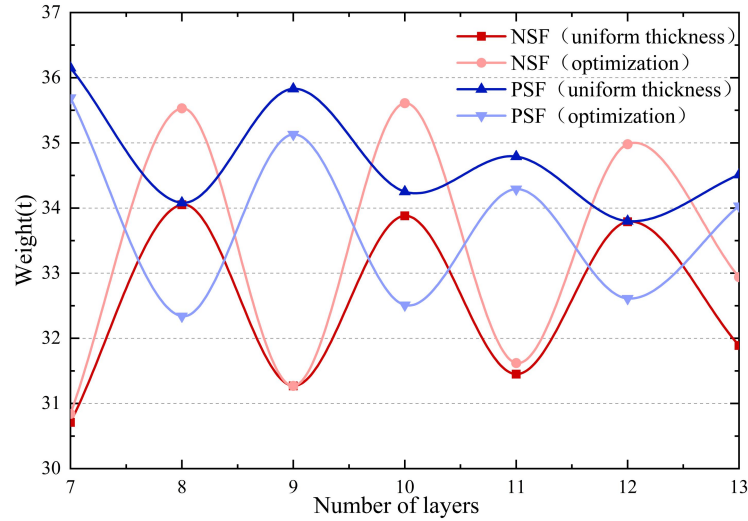
	Layer	Max (mrem/h)				Min (mrem/h)			
		D_{u1}	σ^2	D_{v1}	σ^2	D_{u2}	σ^2	D_{v2}	σ^2
NSF	7	3.42×10^3	2.39×10^{-2}	2.17×10^3	1.95×10^{-2}	1.62×10^3	3.32×10^{-2}	1.03×10^3	2.45×10^{-2}
	8	1.40×10^3	2.62×10^{-2}	1.22×10^3	2.06×10^{-2}	6.02×10^2	4.31×10^{-2}	4.07×10^2	2.56×10^{-2}
	9	2.53×10^3	2.83×10^{-2}	1.36×10^3	2.36×10^{-2}	1.26×10^3	2.13×10^{-2}	6.47×10^2	2.81×10^{-2}
	10	1.25×10^3	2.82×10^{-2}	1.02×10^3	2.67×10^{-2}	5.56×10^2	1.60×10^{-2}	4.11×10^2	3.21×10^{-2}
	11	2.15×10^3	2.68×10^{-2}	1.89×10^3	2.80×10^{-2}	1.07×10^3	1.34×10^{-2}	8.92×10^2	3.44×10^{-2}
	12	1.29×10^3	2.48×10^{-2}	1.09×10^3	2.90×10^{-2}	5.63×10^2	1.29×10^{-2}	3.47×10^2	3.40×10^{-2}
	13	1.84×10^3	2.22×10^{-2}	8.94×10^2	2.72×10^{-2}	9.01×10^2	1.29×10^{-2}	3.86×10^2	3.03×10^{-2}
PSF	Layer	Max (mrem/h)				Min (mrem/h)			
		D_{u3}	σ^2	D_{v3}	σ^2	D_{u4}	σ^2	D_{v4}	σ^2
	7	1.07×10^3	3.32×10^{-2}	9.59×10^2	1.23×10^{-2}	3.90×10^2	2.27×10^{-2}	3.77×10^2	1.60×10^{-2}
	8	2.71×10^3	4.31×10^{-2}	1.50×10^3	1.17×10^{-2}	1.18×10^3	2.25×10^{-2}	6.73×10^2	1.34×10^{-2}
	9	1.04×10^3	2.13×10^{-2}	9.78×10^2	1.13×10^{-2}	4.16×10^2	2.31×10^{-2}	3.85×10^2	1.29×10^{-2}
	10	1.90×10^3	1.60×10^{-2}	1.11×10^3	1.08×10^{-2}	8.49×10^2	2.39×10^{-2}	4.92×10^2	1.29×10^{-2}
	11	1.08×10^3	1.34×10^{-2}	1.04×10^3	1.07×10^{-2}	4.92×10^2	2.34×10^{-2}	4.46×10^2	1.23×10^{-2}
Relative change rate	Relative change rate	$D_{vn} - D_{um}$ / D_{um}							
		$m = 1, n = 1$	$m = 2, n = 2$	$m = 3, n = 3$	$m = 4, n = 4$				
		36.55%	36.42%	10.37%	3.33%				
		12.86%	32.39%	44.65%	42.97%				
		46.25%	48.65%	5.96%	7.45%				
		18.40%	26.08%	41.58%	42.05%				
		12.09%	16.64%	3.70%	9.35%				
Relative thickness distribution of each scheme after optimization	Relative thickness distribution of each scheme after optimization	15.50%	38.37%	0.00%	0.00%				
		51.41%	57.16%	0.00%	2.77%				
		Layer n (from inside to outside)				Relative thickness (cm)			
		1	23.60	20.99	19.24	17.44	15.85	14.70	14.16
		2	20.50	18.57	17.21	15.78	14.50	13.55	13.08
		3	17.40	16.15	15.18	14.12	13.15	12.40	12.00
		4	14.30	13.73	13.15	12.46	11.80	11.25	10.92
		5	11.20	11.31	11.12	10.8	10.45	10.10	9.84
		6	8.10	8.89	9.09	9.14	9.10	8.95	8.76
		7	4.90	6.47	7.06	7.48	7.75	7.80	7.68
		8		3.89	5.03	5.82	6.40	6.65	6.60
		9			2.92	4.16	5.05	5.50	5.52
		10				2.80	3.70	4.35	4.44
		11					2.25	3.20	3.36



(a)



(b)



(c)

Fig. 5 (Color online) Shielding and weight-loss effect analysis before and after optimization:

- (a) Radiation dose rate before and after optimization of two arrangements (NSF).
- (b) Radiation dose rate before and after optimization of two arrangements (PSF).
- (c) Analysis of weight-loss effect before and after optimization.

From Table 2 and Figs. 5(a) and 5(b), if the neutrons are shielded first, the dose rate output by the GA-optimized schemes is significantly lower than the initial series of schemes shown in Fig. 3(a). Furthermore, the maximum value can be reduced by 57%. If the photons are shielded first, as the number of layers increases, the difference between the dose rate obtained by optimization and that obtained by the initial scheme gradually decreases.

The relative thickness distributions of the optimized schemes are summarized in Table 2. Combined with the thickness distribution before and after optimization, the results in Fig. 5 can be divided into two types: the first type: neutrons are shielded first, and the total number of layers is odd; photons are shielded first, and the total number of layers is even; the second type: neutrons are shielded first, and the total number of layers is even; photons are shielded first, and the total number of layers is odd, that is, the two schemes presented at the end of Chapter 2. Considering the results in Table 2 and the particle transport process, most of the particles are absorbed because the shielding layer near the core is thicker. Simultaneously, in the first type of case, because the outermost layer is B₄C, which absorbs some of the remaining neutrons, the relative change rate of the first type of case before and after optimization will be more evident, as shown in Table 2. However, the overall dose level of the first type is higher than that of the second type. Therefore, we did not consider the two cases included in the first type. Also, when the number of layers in Fig. 5(b) increases, the dose before and after optimization does not change, which implies that the relative thickness of each layer decreases, and the absorption capacity of the

corresponding particles worsens. This is similar to the scheme in which each layer is the same thickness.

The weight of each shielding scheme was then calculated, and the results are shown in Fig. 5(c).

Referring to Fig. 3(d), if scheme I is followed, the weight will also be reduced to a certain extent; if scheme II is followed, although the dose is reduced, the weight will be increased to a certain extent. Therefore, we recommend the use of Scheme I. Moreover, relative thickness optimization with GA helps reduce the weight of the shielding layers.

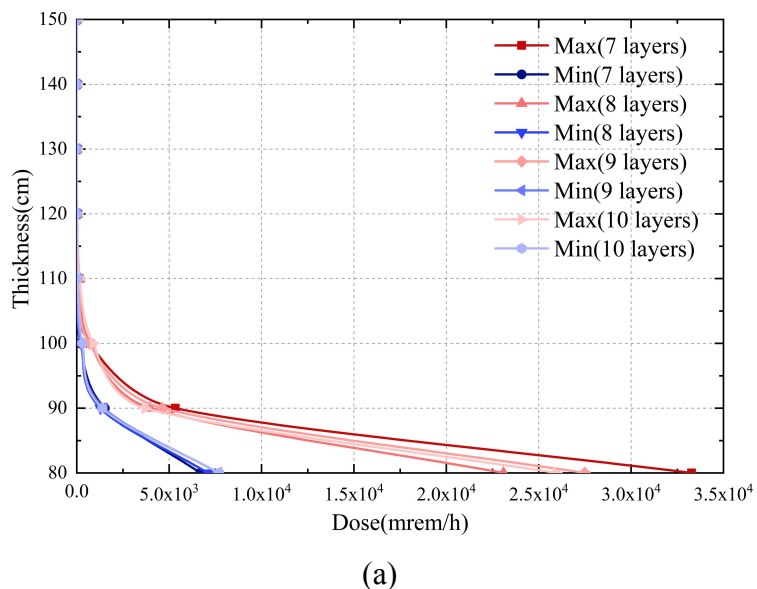
3.2 Determination of total thickness with quantitative correlation

The research results of relevant studies show that when the GA is applied to reactor shielding design, the general method for determining the genetic operators (population size, crossover probability, and mutation probability) is to preset different initial values [26]. Then, appropriate values of the genetic operators are determined by counting the average number of individuals required to achieve the optimal plan under different combinations. Finally, they are inputted into the algorithm framework. The above process involves a large amount of calculation and strong repeatability, which seriously affects the overall efficiency of the shielding design. To avoid repetition of the above process, this section proposes a method for constraining the algorithm directly and quantitatively by providing the total thickness of the shielding layer through the dose.

In this study, the GA-optimized scheme provides the relative thickness of each shielding layer determined according to the design target y in Equation (4). Because the setting of the total weight of the shielding body and dose in y are estimated values, that is, the upper limit of the corresponding value range, any solution within the range that satisfies this value may be regarded as the optimal solution. In addition, the algorithm exhibits the characteristics of a forwarding iteration. It is generally impossible to determine whether the total weight obtained by the sum of the relative thicknesses of each layer is the global optimal solution in the shielding design.

Therefore, the total thickness can be determined by the shielding calculation as the quantitative constraint of the GA optimization process to avoid local optimal solutions [27].

The total thickness is related to the radiation dose requirement. In general, the best approach is to accurately perform Monte Carlo shielding calculations to determine the total thickness based on dose requirements. However, under the condition that the approximate value range cannot be obtained, the process of obtaining ideal results using the Monte Carlo method for the shielding calculation is usually random. To improve the efficiency of the design, we established a quantitative relationship between the total thickness and dose requirements through mass calculations in advance. The total thickness of the shielding layer can be directly determined according to the dose requirements to determine the complete shielding scheme.



(a)

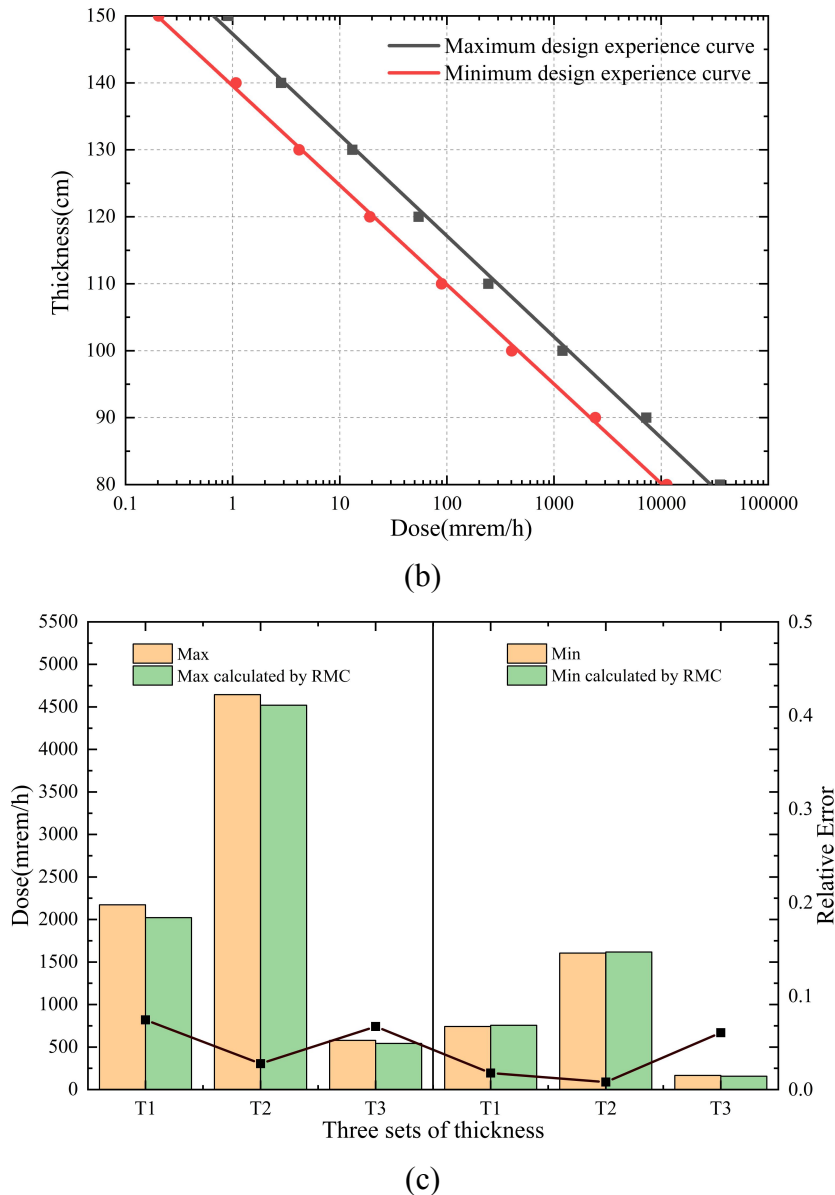


Fig. 6 (Color online) Establishment and validation of quantitative relationships:

(a) Variation of dose with thickness for different shielding layers. (b) Thickness-dose design curve. (c) Comparison of dose values obtained by quantitative equation with those calculated by RMC under different thicknesses (mrem/h).

As shown in Fig. 6(a), the thickness and dose exhibited an exponential change law. The thickness-dose design curves in the logarithmic coordinate system are shown in Fig. 6(b).

We first established a set of equations between the dose rate and total thickness under a constant power (20 MW):

The maximum equation is calculated as follows:

$$T = 148.06 - 15.15D . \quad (7)$$

And the minimum equation is calculated as follows:

$$T = 140.34 - 14.93D . \quad (8)$$

In the equation, T is the total thickness of the shielding layer (cm) and $D = \lg a$, where a = dose (mrem/h).

To verify the calculation accuracy of the above equation, three sets of thicknesses (T_1-T_3) were randomly selected, and the maximum and minimum dose results ($D_{1\text{Max}}-D_{3\text{Max}}$; $D_{1\text{Min}}-D_{3\text{Min}}$) were calculated using Eqs. (7) and (8). T_1-T_3 are substituted as quantitative constraints into the GA toolbox, that is $h_1(x) = T_1$, $h_2(x) = T_2$, $h_3(x) = T_3$. The total shield weight and dose range were set simultaneously. The design variables were entered into the x -dimensional vector space of Eq. (4), and the fitness function was set according to the AHP method. The obtained calculation results, that is, the relative thickness of each layer, together with other design variables, were used as input parameters of the RMC. The results of comparing the dose calculated by RMC with the dose calculated by Eqs. (7) and (8) are shown in Fig. 6(c).

As shown in Fig. 6(c), compared with the results calculated by RMC, the relative error of the extreme values of the dose in all detection areas calculated by Eqs. (7) and (8) is within 10%. The validity and accuracy of the quantitative solution given by the above equation were verified and can be applied to the rapid calculation of the shielding design of small reactors.

Generally, reactors with power levels in the range 5 to 200 MW are referred to as small reactors. Based on the above calculation results, to improve the universality of the equation, the power range was extended to 5–200 MW, and the thickness–dose relationship was specified for the different power levels. This process is illustrated in Fig.7. Under actual design conditions, designers tend to focus on the maximum dose in the detection area; the relationship between the thickness and maximum dose is provided.

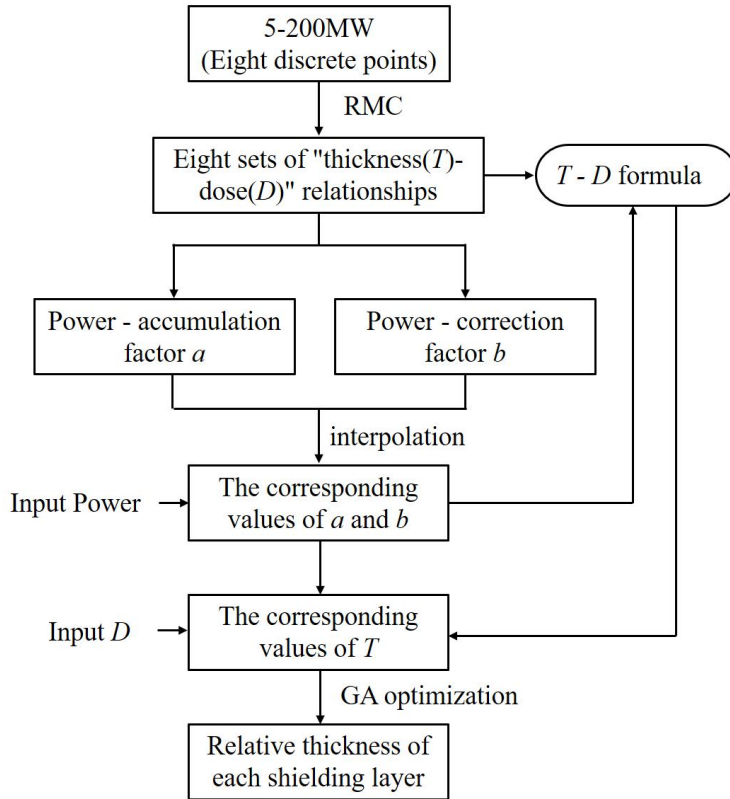


Fig. 7 Flow chart of quantitative shielding design method.

Combined with the conclusions obtained in Chapter 2 and Sect. 3.1, assuming that the particle shielding order is determined, it is evident from Table 2 that when the number of shielding layers is set to 7, the GA-optimized shielding scheme has the smallest dose value compared to those of the other schemes. Therefore, the number of shielding layers was set to 7. The results are shown in Fig. 8.

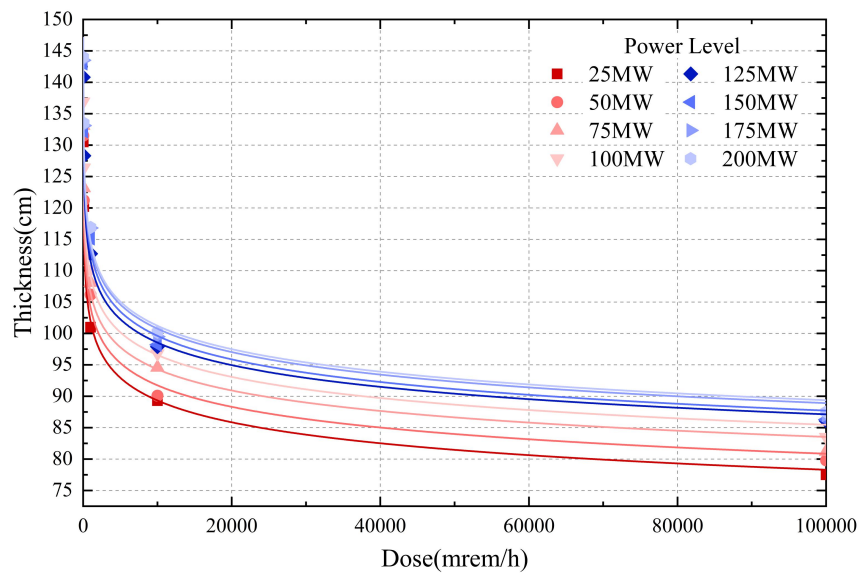


Fig. 8 Thickness-dose relationship curve at different power levels.

As observed, the thickness-dose relationship at different power levels continues to change exponentially. The quantitative relationship can be summarized as follows:

$$T = a \times D^b. \quad (9)$$

As shown in Fig. 7, a represents the dose accumulation factor, and b represents the dose correction factor.

When the design power of the reactor is given, first, the specific values of the accumulation factor a and correction factor b are determined through the relationship between them. Further, a and b are substituted into Eq. (9). Subsequently, the corresponding total thickness of the shielding layer is quantitatively determined according to the dose limit. Combined with the empirical design method and multi-objective optimization method proposed above, the final optimized design scheme can be obtained.

4. EFFECT EVALUATION OF THE METHOD

In this section, the weight-loss effect of the semi-empirical and semi-quantitative shielding design method proposed above is verified, and the method is developed into a shielding design program.

4.1 Evaluation of shielding and weight-loss effect

To verify the effect of the semi-empirical and semi-quantitative shielding design method on radiation shielding and weight reduction of the shielding body simultaneously, we set up three groups of samples for comparison. First, the power of the three groups of samples was randomly set to $P = 37.5$ MW, the dose $D_1 = 100$ mrem/h, and the total thickness of the shielding layer was obtained according to Eq. (9), that is, $T_1 = 119.7$ cm. Further, based on the empirical shielding design method, the shielding body model is established based on Scheme I. The material, number of shielding layers, and initial thickness of each layer were entered as design variables in the GA model contained in Eq. (4). With D_1 and T_1 as quantitative constraints in the optimization process of the GA, corresponding to Eq. (4), $h_1(x) = 100$ and $h_2(x) = 119.7$. Finally, the optimized relative thickness from the

inner to outer radius is shown in Figure 9(a) and Table 3.

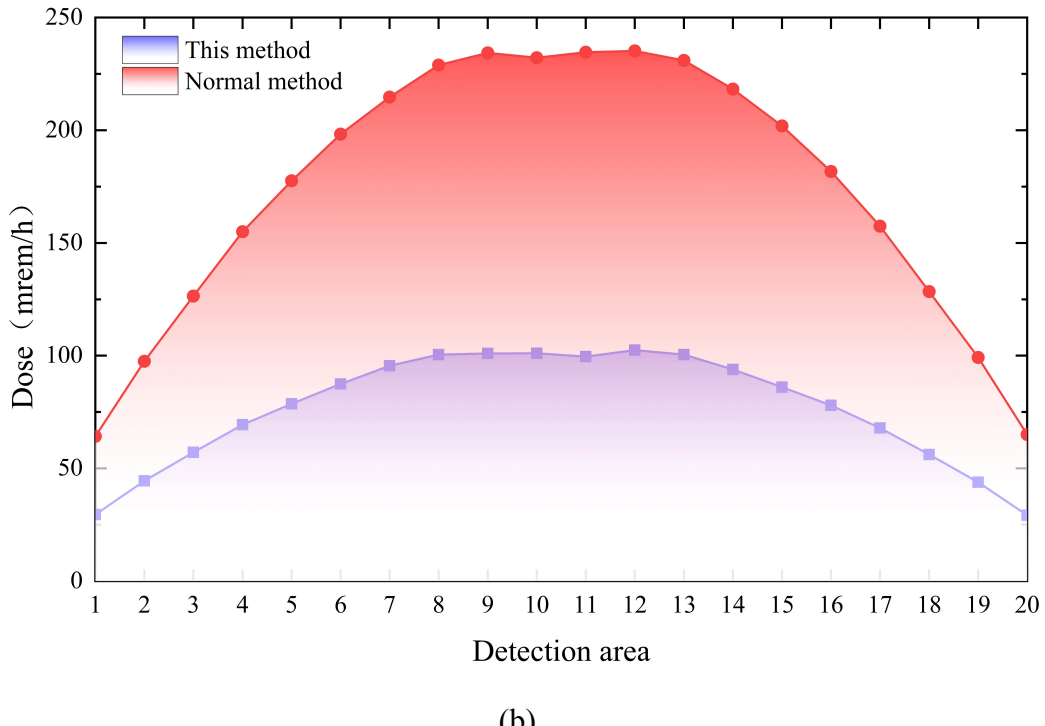
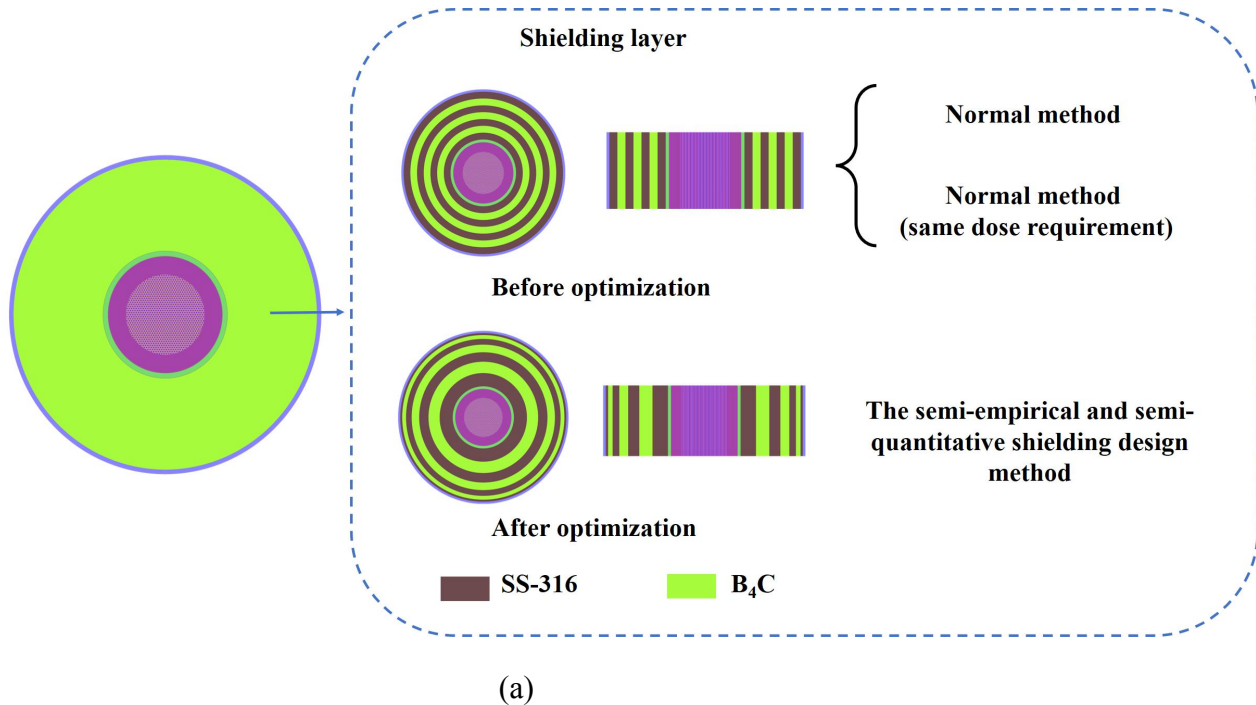


Fig. 9 (Color online) Effect verification. (a) Validation model for shielding and weight-loss effects. (b) Dose comparison between D_2 and D_1 .

Table. 3 Shielding design parameters and calculation results for different schemes

Layer n (from inside to outside)	Relative thickness (cm)			Layer n	Thickness (cm)
	This method	Normal method	Normal method (same dose requirement)		
1	29.7	17.1	18.3		
2	25.5	17.1	18.3		
3	21.3	17.1	18.3	1	68.4
4	17.1	17.1	18.3		
5	12.9	17.1	18.3		
6	8.7	17.1	18.3	2	51.3
7	4.5	17.1	18.3		
Total thickness (cm)	119.7	119.7	128.1		119.7
Total weight (t)	53.52	54.99	60.71		47.08
Maximum dose (mrem/h)	101.04	235.23	100.44		4257.29

Compared with the shielding scheme with equal total thickness, that is, $T_2 = T_1 = 119.7$ cm, and equal relative thickness of each layer, that is, $t_2 = 17.1$ cm, the neutron/photon coupling transport calculation is performed. The total weight of the shielding layer and dose in each detection area of the two schemes are listed in Table 3 and Fig. 9(b). It can be seen that under the condition of the same total thickness, the semi-empirical and semi-quantitative shielding design method can effectively help reduce the radiation dose by approximately 2.3 times. The maximum dose in the detection area decreased from $D_2 = 235.23$ mrem/h to $D_1 = 101.04$ mrem/h. Similarly, as listed in Table 3, when the dose requirements are equal, that is, $D_3 = D_1 = 100$ mrem/h, the semi-empirical and semi-quantitative shielding design method can effectively reduce the total weight of the shielding body from 60.71 t to 53.52 t. This is a reduction difference of 11.84% compared to the normal method (same dose requirement).

In addition, we provide a set of two-layer design schemes. To ensure the same order of particle shielding, SS-316 and B₄C were set up with one layer. The thicknesses of the two layers are given by referring to the scheme in the second

column of Table 3; that is, the sum of the thicknesses of the two layers is 119.7 cm. The maximum dose calculated by this scheme is 4527.29 mrem/h, which is 42 times higher than the scheme optimized by the semi-empirical and semi-quantitative lightweight shielding design method.

To summarize, the power is considered an independent design variable, and the accumulation factor a and correction factor b are derived. Finally, the thickness value was obtained by substituting the two factors into Eq. (9). This method can restrict the total thickness before the specific optimization of the thickness of each layer by the GA. This can effectively avoid determining the local optimal solution owing to its large calculation scale.

4.2 Shield design optimization program SDIC1.0

We encapsulated the semi-empirical and semi-quantitative lightweight shielding design method into SDIC1.0.

The semi-empirical and semi-quantitative lightweight shielding design method is divided into three steps: (1) The number of shielding layers and neutron/photon shielding sequence are determined first by trial calculations, and an empirical scheme is established; (2) The thickness-dose relationship is established through the statistics of mass Monte Carlo calculation results, so as to determine the corresponding total thickness of the shielding layer through the dose requirements, and use this thickness as a constraint to prevent determining a local optimal solution when optimizing the relative thickness of each layer. (3) The relative thickness of the shield layer was optimized by the GA, and the weight of the shield layer was reduced. To encapsulate the semi-empirical and semi-quantitative lightweight shielding design method, we developed the shield optimization design program SDIC1.0. The program process is illustrated in Fig. 10.

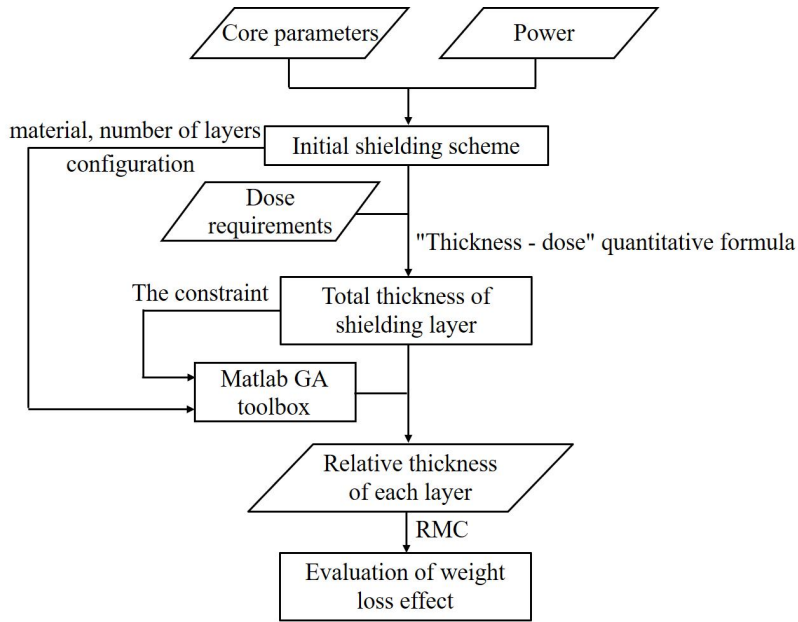


Fig. 10 Process involved in SDIC1.0.

The accuracy of the procedure was verified by randomly setting different groups of power levels and dose limits based on a consistent core scheme. As shown in Table 4, the three groups of random power are 60 MW, 140 MW, and 110 MW, respectively. First, the accumulation factor a and correction factor b were obtained from the input power. Subsequently, three groups of dose limits at different power levels were correspondingly set, that is, $D_1 = 10000$ mrem/h; $D_2 = 5000$ mrem/h; $D_3 = 1000$ mrem/h. The corresponding total thickness of the shielding layer is given according to the dose limits. Furthermore, the content in Sect. 4.1 was repeated, the design variables and constraints were entered, the algorithm was run, and the output, including the relative thickness of each layer, was obtained. Finally, the thickness of each layer optimized by GA was used as the input of the RMC, and the calculated dose was compared with the initially set doses D_1 – D_3 . The results are presented in Table 4.

Table. 4 SDIC1.0 calculation effect verification

Test Data	I	II	III
Power (MW)	60	140	110
a	151.77	164.03	158.99
b	-0.054	-0.055	-0.053
Input dose, D_t (mrem/h)	10000	5000	1000
Total thickness, T_t (cm)	92.38	102.93	110.21
	22.40	24.40	26.02
	19.33	21.17	22.60
	16.26	17.93	19.18
Thickness of each layer(cm)	13.20	14.70	15.76
	10.13	11.46	12.34
	7.10	8.23	8.92
	3.96	5.04	5.39
Dose calculated by RMC D_{rmc} (mrem/h)	10963.36	5520.63	1114.10
Relative error (%)	9.63	10.40	11.40
T_1 (s)	854.16	1272.59	1388.81
T_2 (s)	5413.06	7834.75	9013.71

As shown in Table 4, the relative error between the results of SDIC1.0 and RMC can be effectively controlled at 9.63%, 10.40%, and 11.40%, respectively. By analyzing the reason for the error, it can be speculated that in determining the relationship between power and the two factors a and b , fewer sample points were used, resulting in a certain deviation in the fitting degree between the three. Therefore, in the future, the error caused by the calculation results of the program can be reduced by increasing the density of the initial sample points.

In addition, in terms of the calculation time, as shown in Table 4, T_1 is the time required to obtain the optimal solution using the method proposed in this paper, and T_2 is the time required to obtain a result similar to D_t by simply using the Monte Carlo code RMC. The calculation time can be shortened by approximately 6.3 times by using this method.

5. CONCLUSION

This study investigates the shielding design method of a small helium-xenon reactor. First, an empirical shielding design method is proposed according to the core parameters. Further, guided by the design objective and combined with empirical design methods, the GA is applied to optimize the relative thickness of each layer. The weight-loss effect of the optimized scheme is evaluated and compared with that of the conventional scheme. For the local optimal solution that GA may generate, this study proposes a quantitative design method based on the results of a large-scale Monte Carlo calculation. It can determine the total thickness of the shielding layer according to the power and dose requirements before GA optimization. The total thickness can be used as a quantitative constraint before running the algorithm. Finally, we integrated the above processes and proposed a semi-empirical and semi-quantitative lightweight shielding design method. The semi-empirical and semi-quantitative lightweight shielding design method has certain advantages in terms of shielding and weight-loss effects, computational efficiency, and accuracy. Specific conclusions drawn through each chapter can be summarized as follows:

1. An empirical shielding scheme is proposed: photons are preferentially shielded, and the number of shield layers is set to an odd number.
2. GA optimization can reduce the radiation dose rate to 57%.
3. The thickness-dose relationship under different power levels is given. It has been verified that when combined with empirical methods, the shielding scheme obtained after GA optimization can reduce the weight by 11.84% compared to the conventional scheme.
4. The result was encapsulated to form a shielding design program SDIC1.0. The test results show that under the same masking scheme, the shielding solution error recorded by SDIC1.0 and Monte Carlo software RMC is controlled at approximately 10%, and the time is by 6.3 times in SDIC1.0.

The semi-empirical and semi-quantitative lightweight shielding design method

can quickly determine the shielding scheme and provide an initial scheme for more detailed shielding optimization. A more universal method will be proposed in the future by introducing energy spectrum characteristics and physical characteristics of materials. In addition, this study primarily focuses on the refined design of the radial shielding layer. The axial dose field distribution is significantly different from the radial distribution. Further research on the axial dose-field distribution is necessary to design an axial shielding layer.

Author contributions

All authors contributed to the study conception and design. Material preparation, data collection and analysis were performed by Song-Chuan Zheng and Qing-Quan Pan. Resources and supervision were performed by Huan-Wen Lv, Song-Qian Tang and Xiao-Jing Liu. The first draft of the manuscript was written by Song-Chuan Zheng and all authors commented on previous versions of the manuscript. All authors read and approved the final manuscript.

Data Availability Statement The data that support the findings of this study are openly available in Science Data Bank at [https://www.doi.org/\[数据 DOI 编号\]](https://www.doi.org/[数据 DOI 编号]) and [http://resolve.pid21.cn/\[数据 CSTR 编号\]](http://resolve.pid21.cn/[数据 CSTR 编号]).

REFERENCES

- [1] L. Zhang, M. Jia, J. Gong et al. Overview of Calculation Methods and Codes for Reactor Radiation Shielding. Nuclear Electronics & Detection Technology (in Chinese), 2018, 38(04):516-520.
<https://kns.cnki.net/kcms/detail/detail.aspx?FileName=HERE201804014&DbName=CJFQ2018>
10.3969/j.issn.0258-0934.2018.04.014
- [2] N. M. Schaeffer, Reactor shielding for nuclear engineers. U.S. Atomic Energy Commission Office of Information Services, 1983.
<https://doi.org/10.2172/4479460>
- [3] L. Zhang, B. Zhang, Y. Chen, Spatial Adaptive Algorithm for Discrete Ordinate Shielding Calculation. Atomic Energy Science and Technology (in Chinese), 2018, 52(12):2233-2242.
<https://kns.cnki.net/kcms/detail/11.2044.TL.20181010.1344.002.html>
10.7538/yzk.2018.youxian.0178
- [4] M. Paul, A. D. Ankan, H. Deb et al., A Monte Carlo simulation model to determine the effective concrete materials for fast neutron shielding, Radiation

Physics and Chemistry, Volume 202, 2023, 110476, ISSN 0969-806X
<https://doi.org/10.1016/j.radphyschem.2022.110476>

[5] Y. Qiu, M. Aufiero, K. Wang et al., Development of sensitivity analysis capabilities of generalized responses to nuclear data in Monte Carlo code RMC. Annals of Nuclear Energy, Volume 97, 2016, Pages 142-152.
<https://doi.org/10.1016/j.anucene.2016.07.016>

[6] Q. Pan, J. Rao, S. Huang et al., Improved adaptive variance reduction algorithm based on RMC code for deep penetration problems. Annals of Nuclear Energy, 2020, 137:1-8.
<https://doi.org/10.1016/j.anucene.2019.107113>

[7] H.O. Tekin, T. Manici, Simulations of mass attenuation coefficients for shielding materials using the MCNP-X code. Nucl. Sci. Tech. 28, 95 (2017).
<https://doi.org/10.1007/s41365-017-0253-4>

[8] Q. Pan, T. Zhang, X. Liu et al., SP3-Coupled Global Variance Reduction Method Based On RMC Code. Nucl. Sci. Tech. 32, 122 (2021).
<https://doi.org/10.1007/s41365-021-00973-0>

[9] L. Deng, G. Li, B. Zhang et al. A high fidelity general purpose 3-D Monte Carlo particle transport program JMCT3.0. Nucl. Sci. Tech. 33, 108 (2022).
<https://doi.org/10.1007/s41365-022-01092-0>

[10] R. Li, X. Zhang, S. Liu et al. Research on deep penetration shielding calculation using Monte Carlo particle transport code cosRMC. Atomic Energy Science and Technology (in Chinese) 55(S1), 82-87 (2021).
<https://kns.cnki.net/kcms/detail/11.2044.TL.20210423.1355.026.html>
10.7538/yzk.2020.youxian.0752

[11] C. Cao, P. Cao, Q. Gan, A novel method for rapid calculation of moderated neutron spectrum and its application in deep penetration. Ann. Nucl. Energy 168, 108895 (2022).
<https://doi.org/10.1016/j.anucene.2021.108895>

[12] Q. Pan, N. An, T. Zhang et al., Single-step Monte Carlo criticality algorithm. Computer Physics Communications 279, 108439 (2022).
<https://doi.org/10.1016/j.cpc.2022.108439>

[13] X. Li, Y. Song, J. Mao, Z. Zhang, Many-objective rapid optimization of reactor shielding design based on NSGA – III. Ann. Nucl. Energy 177, 109322 (2022).
<https://doi.org/10.1016/j.anucene.2022.109322>

[14] Z. Chen, Z. Zhang, J. Xie et al. Metaheuristic optimization method for compact reactor radiation shielding design based on genetic algorithm. Ann. Nucl. Energy 134, 318-329 (2019).
<https://doi.org/10.1016/j.anucene.2019.06.031>

[15] Y. Song, Z. Zhang, J. Mao et al. Research on fast intelligence multi-objective optimization method of nuclear reactor radiation shielding. Ann. Nucl. Energy 149, 107771 (2020).
<https://doi.org/10.1016/j.anucene.2020.107771>

[16] Z. Chen, Z. Zhang, J. Xie et al. Multi-objective optimization strategies for radiation shielding design with genetic algorithm. Computer Physics

Communications 260, 107267 (2021).
<https://doi.org/10.1016/j.cpc.2020.107267>

[17] X. Li, W. Li, T. Jiao et al. Component Optimization of Shielding Materials Based on Multi-objective Genetic Algorithm. Annal Report of China Institute of Atomic Energy (in Chinese), 2020(00):111-112 (2020).
<https://kns.cnki.net/kcms/detail/detail.aspx?FileName=FSFH202001015&DbName=CJFQ2020>

[18] X. Wu, Y. Yang, S. Han et al., Multi-objective optimization method for nuclear reactor radiation shielding design based on PSO algorithm. Ann. Nucl. Energy 160, 108404 (2021).
<https://doi.org/10.1016/j.anucene.2021.108404>

[19] Y. Song, J. Mao, Z. Zhang et al. A novel multi-objective shielding optimization method: DNN-PCA-NSGA- II . Ann. Nucl Energy 161, 108461 (2021).
<https://doi.org/10.1016/j.anucene.2021.108461>

[20] S.T. Asbury, Multi-grid genetic algorithms for optimal radiation shield design. University of Michigan, 2012.
<https://www.proquest.com/dissertations-theses/multi-grid-genetic-algorithms-optimal-radiation/docview/1027166861/se-2>

[21] Z. Zhang, S. Zhao, Z. Chen et al, Study on radiation shielding optimization method based on multi-objective evolutionary genetic algorithm. Nucl. Power Engineering _ (in Chinese) 41(S1):124-129 (2020).
<https://kns.cnki.net/kcms/detail/detail.aspx?FileName=HDLG2020S1026&DbName=DKFX2020>
10.13832/j.jnpe.2020.S1.0124

[22] S. Treană, M.A. Jiménez, T. Antczak, A necessary and sufficient condition on the equivalence between local and global optimal solutions in variational control problems. Nonlinear Analysis 191, 111640 (2020).
<https://doi.org/10.1016/j.na.2019.111640>

[23] W. Jiang. To investigate the mechanism of ant colony algorithm to solve the local optimal. Intelligent Computer and Applications. (in Chinese) 4(03):53-54, 59 (2014).
<https://kns.cnki.net/kcms/detail/detail.aspx?FileName=DLXZ201403015&DbName=CJFQ2014>
10.3969/j.issn.2095-2163.2014.03.014

[24] X. Yao, Y. Liu, G. Lin, Evolutionary programming made faster. IEEE T. Evolutionary Computation 3(2), 82-102 (1999).
doi: 10.1109/4235.771163.

[25] Z. Wu, S.J. Hsieh, J. Li, Sensor deployment based on fuzzy graph considering heterogeneity and multiple-objectives to diagnose manufacturing system. Robotics and Computer-Integrated Manufacturing 29, 192-208 (2013).
<https://doi.org/10.1016/j.rcim.2012.05.004>

[26] S. Yang, Research on the intelligent radiation shielding design method using the genetic algorithm. North China Electric Power University, 2012. (in Chinese)

https://kns.cnki.net/kcms2/article/abstract?v=3uoqIhG8C447WN1SO36whHG-SvTYjkCc7dJWN_daf9c2-IbmsiYfKooOoHjsFfe_W2iqf9AXDEUF1Yba2z9YNSKw4tdCKVwN&uniplatform=NZKPT
10.7666/d.y2139659

[27] Y. Lei, S. Zhang, X. Li et al, MATLAB genetic algorithm toolbox and application. Xidian University Press, 2014 (in Chinese)
<https://www.wenkunet.com/d-6558574.html>